Incipient plasticity during nanoindentation at grain boundaries in body-centered cubic metals

Soer, WA; Aifantis, KE; De Hosson, J.T.M.

Published in:
Acta Materialia

DOI:
10.1016/j.actamat.2005.07.001

Publication date:
2005

Available online at www.sciencedirect.com
SCIENCE DIRECT®
Acta Materialia 53 (2005) 4665–4676
Acta MATERIALIA
www.actamat-journals.com

Incipient plasticity during nanoindentation at grain boundaries in body-centered cubic metals

W.A. Soer, K.E. Aifantis, J.Th.M. De Hosson *

Department of Applied Physics, Materials Science Center and the Netherlands Institute for Metals Research, University of Groningen, Nijenborgh 4, 9747 AG Groningen, The Netherlands

Received 8 April 2005; received in revised form 28 June 2005; accepted 1 July 2005
Available online 18 August 2005

Abstract

The mechanical response to nanoindentation near grain boundaries has been investigated in an Fe–14%Si bicrystal with a general grain boundary and two Mo bicrystals with symmetric tilt boundaries. In particular, the indentations performed on the Fe–14%Si show that as the grain boundary is approached, in addition to the occurrence of a first plateau in the load versus depth nanoindentation curve, which indicates grain interior yielding, a second plateau is observed, which is believed to indicate dislocation transfer across the boundary. It is noted that the hardness at the onset of these yield excursions increases as the distance of the tip to the boundary decreases, providing thus a new type of size effects, which can be obtained through nanoindentation. The energy released during an excursion compares well to the calculated interaction energy of the piled-up dislocations. Hall–Petch slope values calculated from the excursions are consistent with macroscopically determined properties, suggesting that the Hall–Petch slope may be used to predict whether slip transmission occurs during indentation. No slip transmission was observed in the Mo bicrystals; however, the staircase yielding commonly found during initial loading was suppressed in the proximity of a grain boundary due to preferential dislocation nucleation at the boundary. An estimate for the nucleation shear stress at the boundary was obtained from the measured interaction range.

Keywords: Nanoindentation; Grain boundaries; Yield phenomena; Slip

1. Introduction

Subgranular microhardness testing has been used for a long time to probe grain boundary hardening effects due to solute segregation in polycrystalline materials [1,2]. Hardening in these experiments is typically found up to tens of micrometers from the grain boundary. In the absence of solute or vacancy gradients near the boundary, no hardening is observed at this scale. The possibility to measure an intrinsic hardening contribution of the grain boundary, as a result of the difficulty in slip transmission across the boundary, has recently come under investigation with the widespread availability of the nanoindentation technique. Low-load indentation experiments [3,4] have shown significant hardening effects within a distance of the order of 1 μm from the boundary. Such experiments could potentially offer detailed information about the intrinsic mechanical properties of individual grain boundaries. So far however, a thorough understanding of the mechanical response is lacking.

Recent studies [4,5] have shown that nanoindentation measurements in the direct proximity of grain boundaries in body-centered cubic (bcc) metals show typical yield excursions under certain conditions. Based on the indentation load and depth at which these excursions

* Corresponding author.
E-mail address: j.t.m.de.hosson@rug.nl (J.Th.M. De Hosson).

1359-6454/$30.00
doi:10.1016/j.actamat.2005.07.001

are observed, it was proposed that they are strain bursts due to dislocation pile-up and subsequent transmission across the boundary. This paper presents new results supporting this perception and providing predictive criteria for strain bursts to occur.

Nanoindentation is frequently employed to investigate the mechanical behavior of materials that have submicrometer scale features or constraints [6]. Significant size effects on the initial elasto-plastic behavior have been observed during indentation of structures that are constrained to such a scale [7]. In the present experiments, the deformed volume is limited to a submicron length scale by the indenter on the one side and the grain boundary on the other side, resulting in a significant size effect on the observed strain bursts. In this new type of size effect, the hardness at which the excursion occurs increases as the indenter tip to boundary distance decreases. Furthermore, it is shown that also in the absence of strain bursts, the indentation experiments provide valuable information on the incipient plastic behavior of the boundary and on the nature of the interaction between the boundary and the indentation-induced dislocations.

2. Experimental procedure

The measured indentation behavior of a grain boundary in general may be affected by many microstructural and geometrical parameters, such as the presence of second phases, gradients in solute or defect concentrations, the inclination of the boundary plane, the curvature of the boundary, the presence of triple junctions and the surface topology at the boundary. Therefore, in order to isolate the intrinsic indentation response of an individual grain boundary, bicrystalline or at least coarse-grained single-phase specimens are required. In this study, one Fe–14%Si alloy bicrystal with a general grain boundary and two pure Mo bicrystals with symmetric coincident site lattice (CSL) ⟨1 1 0⟩ tilt boundaries were used, all of which were prepared by floating-zone melting. The geometrical parameters are summarized in Table 1. The Fe–Si specimen contained traces of phosphorus and carbon [8]. Auger spectroscopy showed no detectable impurities on the grain boundaries in the Mo bicrystals [9,10].

The specimen surfaces were polished using a final polishing colloidal silica suspension. For the Mo bicrystals, 96 ml of the suspension was mixed with 2 ml ammonia solution (25%) and 2 ml hydrogen peroxide solution (30%). By atomic force microscopy it was confirmed that no severe preferential grain boundary attack resulted from these additives. Over a lateral distance of 30 μm across the boundary, a smooth height profile with a maximum slope of less than 0.2° was found, which is not expected to influence the local indentation response. Electron backscatter diffraction (EBSD) was employed to locate the grain boundaries with respect to a grid of marker indents.

Nanoindentation measurements were carried out employing an MTS Nano Indenter XP (MTS Nano Instruments, Oak Ridge, TN) with a pyramidal Berkovich tip using the continuous stiffness measurement (CSM) technique [11]. Load-controlled indentations were made to a maximum depth of 200 nm with a targeted strain rate of $0.05\ s^{-1}$, which corresponds to a maximum loading rate of the order of 0.1 mN/s. The azimuthal orientation of the indenter was chosen to have one side of the triangular impression of the Berkovich tip parallel to the grain boundary under investigation. In order to vary the distance to the boundary with the smallest possible increments, lines of indentations were drawn across the grain boundary at angles smaller than 3° with a spacing of 3 μm between the indents. Although the plastically deformed zones of consecutive indents are likely to overlap at such close spacing, no significant effect of any crosstalk interaction on the measured response was found in a test comparing lines of indents of 200 nm depth with spacings ranging from 3 to 10 μm in the Fe–Si matrix. This is possibly due to a slight work hardening introduced by mechanical polishing of the surfaces, compared to which the additional hardening effect from adjacent indentations is very small.

3. Results

3.1. Load–displacement response

Results for the Fe–Si bicrystal were obtained from four lines of 60 indentations crossing the grain boundary. Initial yielding was evidenced in all indentations by a displacement excursion at a constant load of around 50 μN. In each of the lines, two or three consecutive indentations which were crossing the boundary, as shown in Fig. 1, exhibited a characteristic yield excur-

Table 1
Grain boundary parameters and indentation direction in crystal coordinates

Specimen	Material	Misorientation	Boundary plane	Indentation direction
1	Fe–14%Si	[−0.29 0.12 0.03] Rodrigues vector	$(-0.75\ 0.56\ 0.35)_A//(-0.89\ 0.44–0.14)_B$	$[0.34–0.13\ 0.93]_A//[0.05\ 0.40\ 0.91]_B$
2	Mo	Σ3	$(\bar{1}\ 2\ 1)_A//(1\ 2\ \bar{1})_B$	$[1\ 0\ 1]_A//[1\ 0\ 1]_B$
3	Mo	Σ11	$(\bar{3}\ 2\ 3)_A//(3\ 2\ \bar{3})_B$	$[1\ 0\ 1]_A//[1\ 0\ 1]_B$

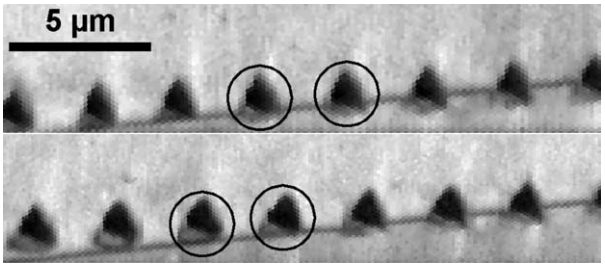

Fig. 1. EBSD scans of two lines of indentations crossing the grain boundary in the Fe–Si bicrystal. The gray scale values represent the quality of the Kikuchi pattern. The circled indentations showed one or two yield excursions as illustrated in Fig. 2.

sion well beyond the initial yield plateau. The excursions were observed for a total of nine measurements located within 0.74 μm of the boundary and only when one side of the indenter was facing the boundary. Although most of these indents crossed over the boundary at maximum indentation depth, it is readily concluded from the load–displacement data that the indenter was still well away from the boundary at the instant of the excursion, at distances ranging from 0.11 to 0.34 μm. It should be emphasized that this behavior was not found for any of the indentations in the matrix, but also not all indents crossing the boundary displayed such a burst. Two types

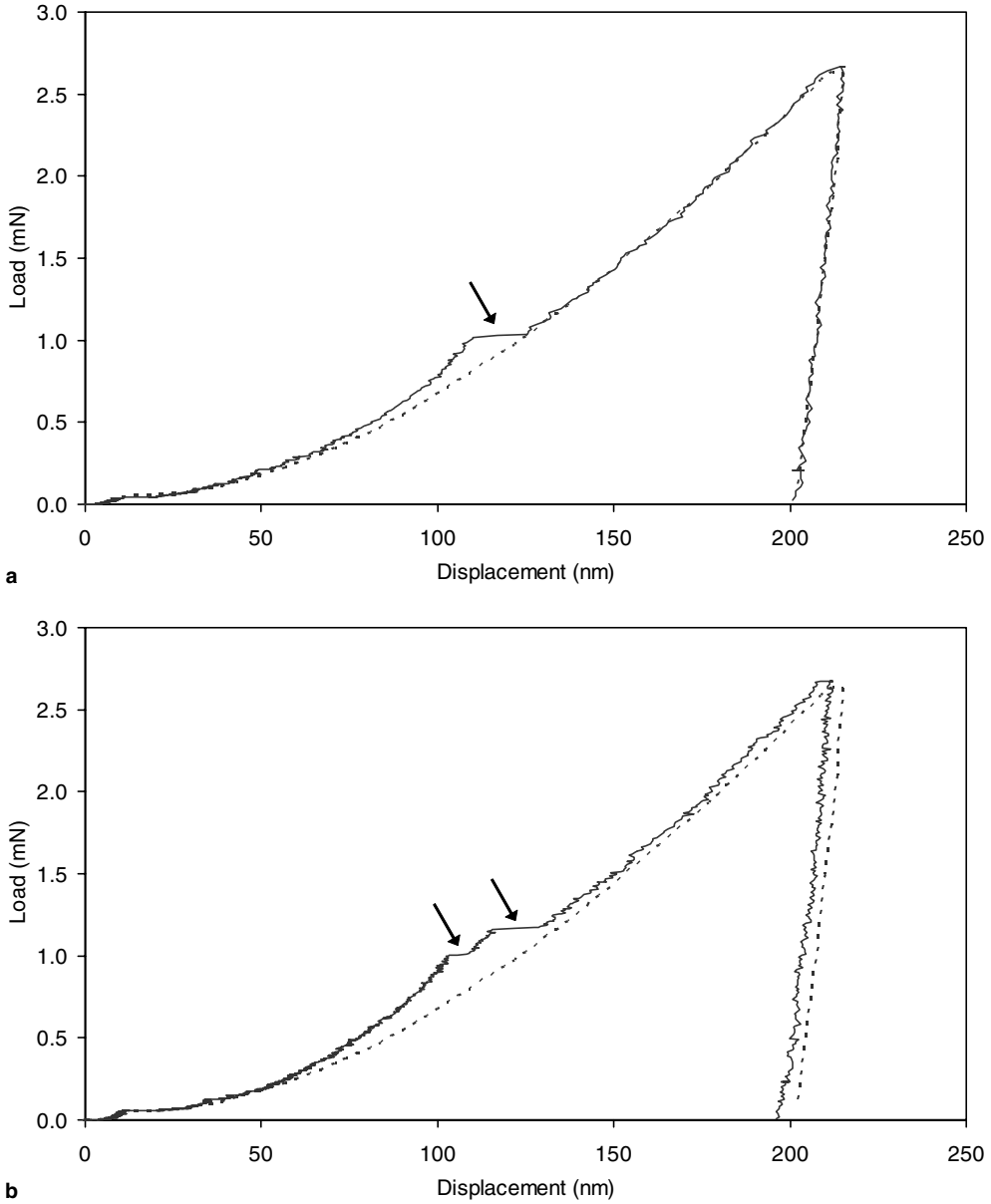

Fig. 2. Indentation response near the Fe–Si grain boundary showing (a) one yield excursion, and (b) two yield excursions (marked with arrows). The dashed line represents the bulk response, which was calculated by averaging six load–displacement curves of indentations in the grain interior.

Table 2
Indentation data for observed yield excursions (bursts) at the boundary in the Fe–Si bicrystal; "1st" and "2nd" entries denote indentations that showed two separate bursts

Line	Indent	Initial distance to boundary d_{center} (nm)	Distance to boundary at onset of burst d_{burst} (Nm)	Load at onset of burst P (mN)	Depth at onset of burst h (nm)	Length of burst Δh (nm)	CSM hardness before burst H (GPa)
1	1	493	210	1.24	130	11	3.20
	2	370	131	1.02	110	16	3.70
2	1	665	335	1.67	152	10	3.17
	2	517 1st	223	1.39	135	4	3.33
		2nd	189	1.79	151	20	
3	1	597	169	2.83	197	19	3.20
	2	463 1st	146	1.52	146	4	3.17
		2nd	109	1.88	163	13	
	3	330 1st	106	1.01	103	6	4.25
		2nd	78	1.16	116	13	
4	1	740	310	2.58	198	9	2.68
	2	555	196	1.91	165	12	2.88

of yield behavior can be distinguished. In six of the nine indentations, the material yielded in one displacement burst at constant load, as shown in Fig. 2(a); the other three curves show two distinct bursts, which are separated by a loading portion, as in Fig. 2(b). A summary of the indentation parameters at the yield excursions is given in Table 2.

On both Mo bicrystals, results were obtained from three lines of 60 indents across the boundary. The initial yield behavior of the Mo grain interior showed multiple yield excursions up to a load of around 1.5 mN, rather than a single yield point as observed in the Fe–Si grain interior. In these excursions, the indentation depth suddenly increased by typically tens of nanometers at constant load. A significant effect of the boundaries on this so-called staircase yielding was found, as shown in Fig. 3. Indentations made within 0.2 μm of the Σ3 boundary showed only very small excursions of less than 10 nm, and in some cases, the deformation appeared to be plastic at the onset of contact and no excursions were found altogether. For indentations further from the boundary, the excursions rapidly become more pronounced, as illustrated by the initial loading response of four subsequent indentations plotted in Fig. 4. Beyond 0.3 μm from the boundary, the load at which the excursions occur seems to be arbitrary and shows no correlation with the distance to the boundary. A similar but less pronounced effect was observed at the Σ11

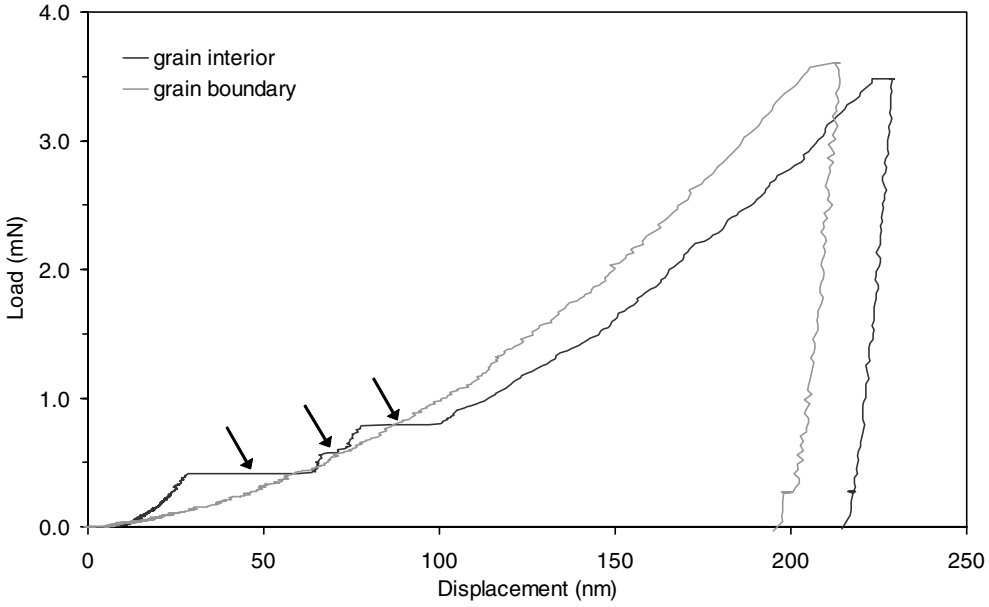

Fig. 3. Load vs. displacement curves recorded in the Mo grain interior and close to the coherent Σ3 boundary. The yield excursions in the grain interior are marked with arrows. In the indentation near the boundary, the yield excursions are suppressed.

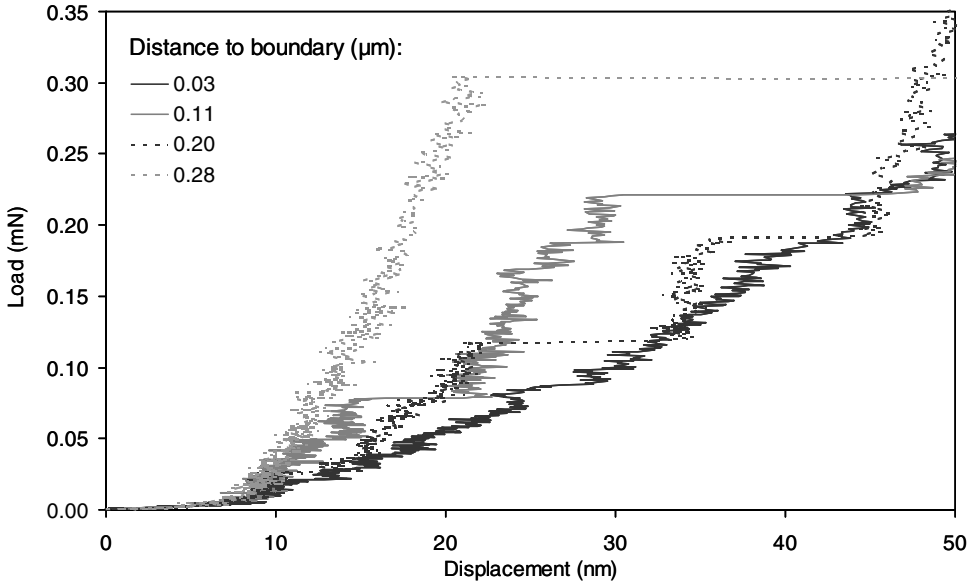

Fig. 4. Initial loading response of four consecutive indentations close to the Mo Σ3 boundary. At 0.03 μm from the boundary, loading appears to be plastic from the onset of contact and no yield excursions are found. With increasing distance, the initial loading approaches elastic behavior and the subsequent yield excursions rapidly become more pronounced.

boundary. In this case, excursions were present in all indentations at the interface, including the ones that showed immediate plastic contact. Besides initial yielding, neither of the two Mo bicrystals showed characteristic displacement bursts near the boundary at higher loads as observed in the Fe–Si specimen.

3.2. Grain boundary hardening

Hardness profiles across the grain boundaries were calculated using hardness values from the continuous stiffness measurement averaged from 80 to 200 nm indentation depth. The values thus represent the hardness experienced by the indenter over this entire range, rather than at the maximum indentation depth [11]. This allows the contribution from the observed non-linearities in the indentation response to be included in our hardening analysis. Due to the commonly observed indentation size effect [12], the CSM hardness decreases continuously with increasing indentation depth. An additional depth dependence of the hardness may be presented by the work hardening introduced by mechanical polishing. Since neither of these depth dependences is expected to be correlated to the presence of a grain boundary, we can use the hardness values of indentations with the same indentation depth to construct a hardness profile. For both Fe–Si and Mo, we found that at 80 nm indentation depth, the hardness had come within approx. 15% of the hardness measured at 200 nm.

Fig. 5 shows the hardness profiles of the investigated boundaries. All three bicrystals showed a significant hardness peak within 1 μm of the boundary. The maximum hardness in Fe–Si was attained around 0.3 μm from the boundary and only to the side where the yield excursions were observed. In both Mo bicrystals, however, the peak hardness coincides with the boundary. Immediately following the peak, a local minimum of the hardness was observed on both sides of the Fe–Si and Mo Σ3 boundaries and on one side of the Mo Σ11 boundary. The hardness on the other side of the Mo Σ11 boundary decreased more gradually to the grain interior value.

4. Discussion

4.1. Dislocation–boundary interaction during slip transmission

As illustrated in Fig. 2, all indentations in the Fe–Si bicrystal exhibited an initial yield excursion at around 10 nm indentation depth, including those at the grain boundary. This yield phenomenon has been attributed to the nucleation or multiplication of dislocations [13,14], and in other cases to the escape of piled-up dislocations to the free surface upon the fracture of the native oxide [15]. While the present results cannot rule out any particular mechanism, it is clear that the observed yielding at higher loads is strongly related to the presence of the grain boundary and can therefore not be explained by these concepts; the purpose of the following analysis is to justify the assumption that this second plateau indicates dislocation transfer across the boundary.

Comparing the curve showing a yield excursion to the bulk response in Fig. 2(a), it is readily found that there is quite an amount of extra elastic energy stored near the

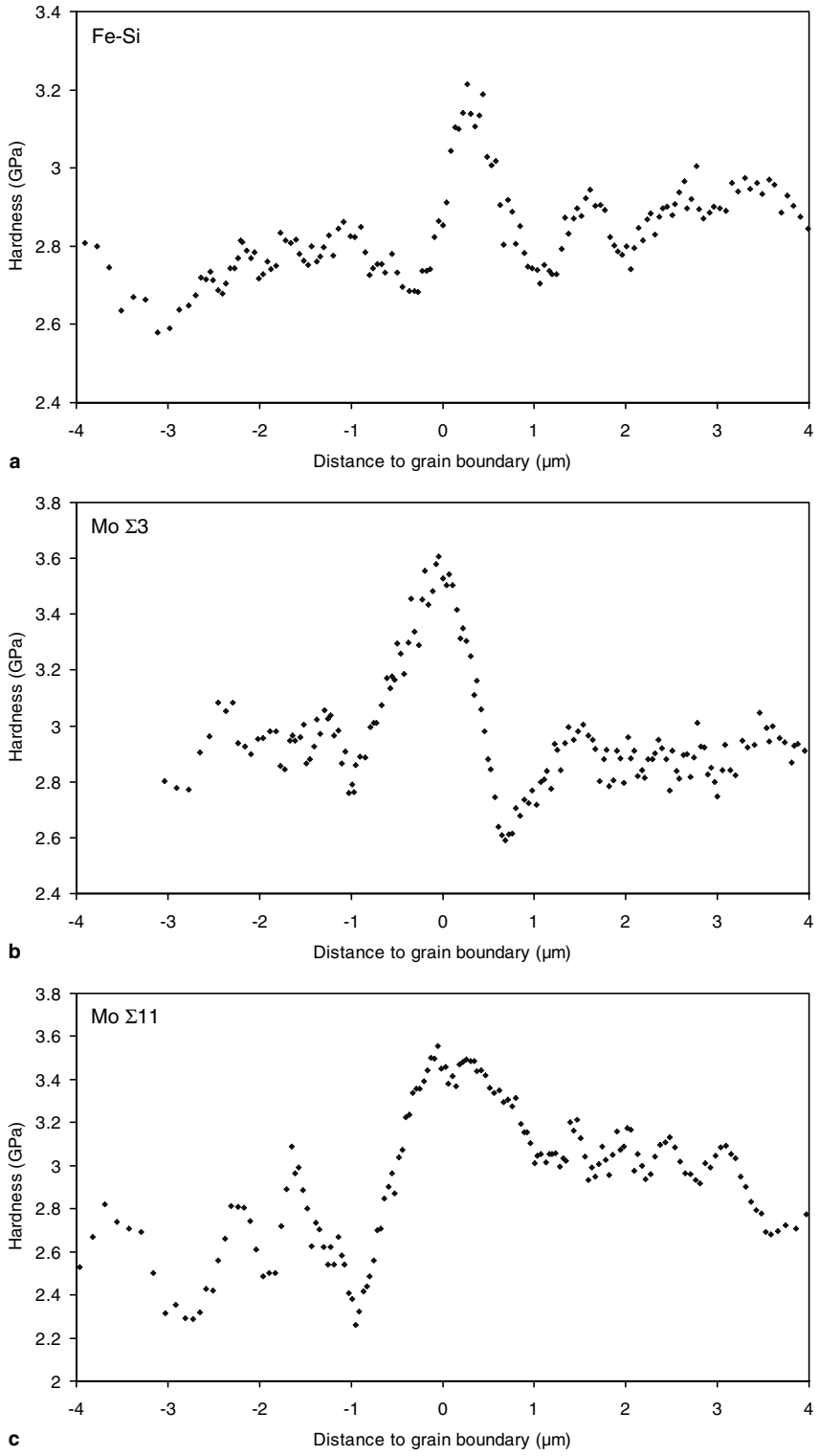

Fig. 5. CSM hardness profiles across (a) Fe–Si, (b) Mo Σ3 and (c) Mo Σ11 boundaries. The data points represent a moving average over five measurements of both hardness and distance. A positive distance to the boundary corresponds to an orientation where one side of the indenter impression faces the grain boundary; for negative distances, an apex of the impression points towards the boundary.

boundary prior to the excursion. The excess of stored energy W_{GB} is given by the area between both curves up to the onset of the excursion and is computed from the graphs to be 8×10^{-12} J. It is of interest to investigate whether this amount of energy can be accounted for by a dislocation-based mechanism, in particular by

dislocation pile-up and transmission at the boundary as proposed earlier [4].

Let us assume that a dislocation pile-up experiences an applied shear stress of $\tau_a = 600$ MPa as given by the experiments; the applied shear stress at the excursion is approximately one-sixth of the recorded hardness. The length of a dislocation pile-up under an applied shear stress is formulated as:

$$l_{\text{pile-up}} = \frac{\mu b n}{\pi \tau_a} \tag{1}$$

where n is the number of dislocation loops in the pile-up, ignoring the difference between edge and screw parts. From Table 2, the distance from the indenter to the grain boundary at the onset of the burst is estimated to be of the order of 300 nm, and therefore Eq. (1) gives that n is approximately equal to 25. The stress fields of a stressed dislocation pile-up of 25 dislocations have been calculated based on linear elasticity. Under an applied shear stress of τ_a, the positions of the edge dislocations in the pile-up with the first dislocation locked at $x = 0$ are given by

$$\sum_{i,i\neq j}^{N-1} \frac{\mu b}{2\pi(1-\nu)} \frac{1}{x_j - x_i} + \tau_a = 0. \tag{2}$$

It can be shown that the position x_i of the dislocations are given by the zeros of the polynomial

$$g(x) = \prod_{i=1}^{N-1} (x - x_i), \tag{3}$$

where $g(x)$ is the first derivative of the Nth Laguerre polynomial [16,17]:

$$g(x) = L'_N\left(\frac{4\pi(1-\nu)\tau x}{\mu b}\right). \tag{4}$$

The calculations provide the position of each of the 25 dislocations with respect to each other, which can be used to compute the total energy of the dislocation burst, i.e., the excursion in Fig. 2(a). The theoretical prediction of the length of the burst is equal to n times the Burgers vector b, which is of the same order of magnitude as experimentally observed (see Table 2).

Because the positions of the dislocations in the stressed pile-up are known, the elastic energy stored in the 25 dislocation loops near the spearhead of the pile-up can be predicted from

$$E_t = \sum_i E_i^{\text{self}} + \sum_p \sum_q E^{\text{I}}(r_{pq}) \tag{5}$$

It turns out that the self energy of the leading 25 dislocation loops of radius 300 nm is far less than the interaction energy among the dislocation loops, i.e., 5.8×10^{-14} and 5.1×10^{-12} J, respectively. This was also found in [18] for indentation of thin films. Comparison with the experimentally determined value for W_{GB} of 8×10^{-12} J leads to the conclusion that there is a fair agreement with E_t and that the plateau observed in the load–displacement curves can be attributed to the release of dislocations in the pile-up in front of the boundary.

In the release of the pile-up into the adjacent grain, several mechanisms may be active, including direct transmission across the boundary (for screw components if the slip planes in both grains intersect the boundary in a common line), absorption by dissociation in the boundary, and dislocation absorption and subsequent re-emission [19]. In the light of our observation of two separate excursions (Fig. 2(b)), the latter mechanism is believed to be predominant. Indeed other mechanism are possible, e.g., subsequent slip on two different slip planes or slip systems but considering Schmid factors as a first approach in previous experiments [4] we did not find clear indications for multiple slip. At the first excursion, dislocations are absorbed into the grain boundary and pile-up at a boundary step. With increasing load, this pile-up produces a stress high enough to nucleate dislocations in the adjacent grain, thereby causing a second yield excursion. This mechanism is illustrated in Fig. 6. Since the extent of dislocation absorption by the boundary depends on the local density of grain boundary dislocations and steps, the corresponding burst may vary in size or be absent altogether, as for the indentations showing only one excursion. The possible presence of segregated impurities may provide additional obstacles to grain boundary dislocations or easy sites for nucleation in the adjacent grain. However, this is not expected to change the observed behavior in a qualitative sense.

The proposed mechanism of dislocation absorption and re-emission is supported by in situ transmission electron microscopy studies of slip propagation across boundaries in bcc metals [20–22]. In some cases, dislocations were found to stop at a short distance from the grain boundary and cross-slip into a plane nearly parallel to the boundary [23]. Because of the non-planar core structure of screw dislocations [24,25], non-Schmid behavior is observed [26] and dislocation pile-ups rarely occur during macroscopic deformation. In the present case, however, the movement of dislocations is confined to a small volume and it can therefore be assumed that some extent of pile-up exists. It is furthermore likely that dislocations pile-up on multiple parallel slip systems. The existence of multiple pile-ups and their interaction are not included in our energy calculation as it serves only to compare the energies to a first approximation.

4.2. Dislocation–boundary interaction in the absence of slip transmission

The initial yielding of the Mo grain interior markedly differs from the behavior observed in Fe–Si in two aspects. Firstly, rather than a single yield excursion, the

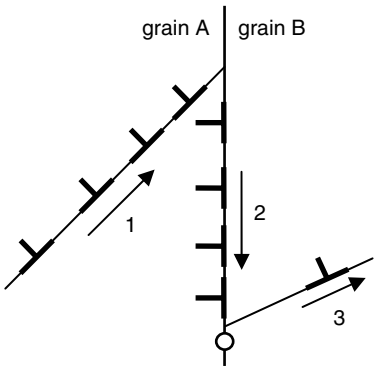

Fig. 6. Schematic of proposed mechanism for slip transmission, showing pile-up of lattice dislocations at the boundary (1), absorption by the boundary and pile-up of grain boundary dislocations at an obstacle (2), and emission into the adjacent grain (3).

loading curve shows multiple yield excursions separated by purely elastic loading portions [27]. This type of behavior may be explained in terms of a (super)dislocation model driven by the change in shear stress from elastic loading to fully plastic indentation [14]. Staircase yielding occurs if the shear stress prior to yield is only slightly higher than the flow stress, so that upon yielding, the shear stress drops below the nucleation shear stress and further elastic loading is needed to reactivate dislocation sources. This process repeats until fully plastic loading is established. Secondly, the loads at which the excursions occur vary considerably throughout the grain interior. This is thought to be mainly due to variations in dislocation density and surface stresses introduced by mechanical polishing of the surface. Oxide films are not expected to play a significant role as molybdenum does not oxidize appreciably at room temperature.

The loading response prior to the initial yield point is well described by purely elastic loading [28]. The maximum elastic shear stress τ_{max} under a rounded Berkovich indenter can be approximated by the relation for a spherical indenter with the same tip radius R [29]

$$\tau_{max} = 0.31\left(\frac{6PE^{*2}}{\pi^3 R^2}\right)^{1/3}, \quad (6)$$

where P is the indentation load and E^* is the reduced modulus of the indenter and the specimen. In our experiments, the first yield point occurred at loads ranging from 0.1 up to 0.6 mN. With an estimated tip radius of 200 nm, the maximum shear stress under the indenter at a load of 0.6 mN is found to be of the same order as the theoretical shear strength of molybdenum $\tau_{th} \approx \mu/2\pi = 20$ GPa. Evidently, the absence of an existing dislocation field is not a prerequisite to attain values close to this shear stress, as was observed earlier for indentation of tungsten single crystals [14]; the investigated surfaces were mechanically polished and hence contained many dislocations. The perception that dislocations may exist or be nucleated prior to the first yield excursion is supported by atomistic simulations of indentation of Mo (1 0 0) and (1 1 1) surfaces [30].

The absence of observable grain boundary yielding in the Mo bicrystals can either be due to the boundary yield stress being too low, in which case no dislocation pile-up can be sustained at the boundary, or too high, so that the pile-up cannot be transmitted across the boundary. The fact that significant hardening is observed suggests that dislocations do pile-up at the boundary, but the shear stress at the spearhead is not sufficient to initiate emission into the adjacent grain. Following the hardening regime, significant softening with respect to the grain interior is found between roughly 0.5 and 1.0 μm from the boundary. This may be explained by the elastic interaction between induced lattice dislocations and the grain boundary [31,32], which may be either attractive or repulsive; an attractive force on the outer dislocation loops around the indenter may lead to apparent softening in the indentation response.

The observed attenuation of grain interior yield excursions for indentations near the grain boundaries is presumably caused by preferential nucleation of dislocations at the boundary. This phenomenon has been considered by Lilleodden et al. [33], who performed atomistic simulations of grain boundary proximity effects on the indentation behavior of gold thin films. It was found that indentation by a 40 Å radius indenter within 25 Å of a Σ79 tilt boundary leads to a significant reduction of the critical load for initial yielding. In the present experiments, the indenter radius is two orders of magnitude larger, and a boundary proximity effect was therefore measured at accordingly larger distances. Up to 0.3 μm from the Mo Σ3 boundary, initial yielding occurs at significantly lower loads than away from the boundary as shown in Fig. 7. Beyond this distance, dislocations nucleate in the grain interior at varying loads depending on the local density of statistically stored dislocations.

From the interaction range of 0.3 μm, an estimate for the nucleation shear stress of dislocations at the boundary can be obtained. In order for dislocations to nucleate from the boundary, the nucleation shear stress must be attained at the boundary before grain interior yielding occurs according to Eq. (6) . Using the two-dimensional analytical solution for the elastic stress fields under cylindrical contact [29] for an indenter radius of 200 nm and a load of 0.6 mN, we find that the maximum shear stress at a lateral distance of 300 nm from the indenter is approximately 2 GPa. As expected, this value for the nucleation shear stress is considerably lower than the theoretical shear stress. The transition from nucleation at the boundary to nucleation in the grain interior was less clear for the Σ11 boundary; therefore, the nucleation stress has not been calculated for this case. It should be noted that the ease of dislocation

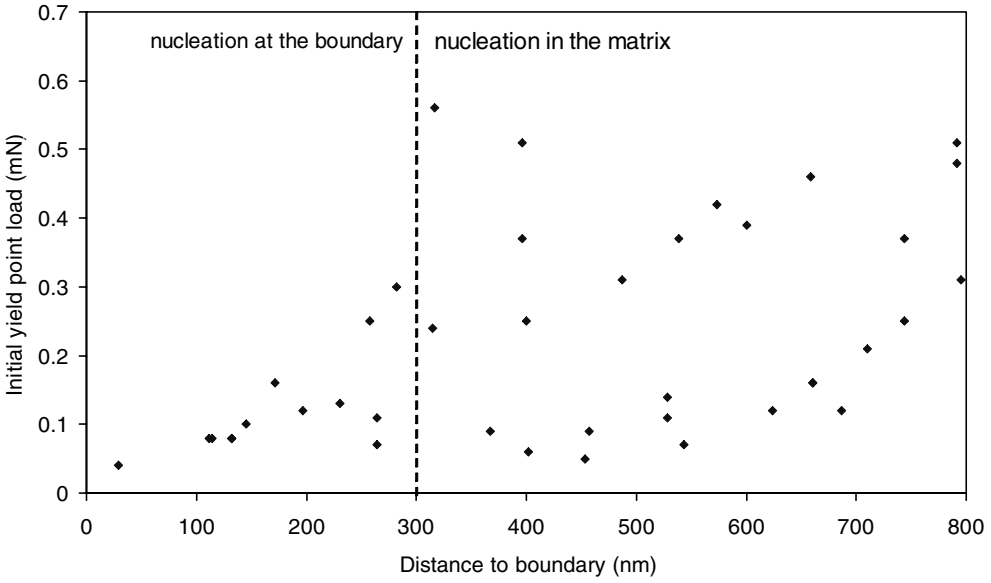

Fig. 7. Correlation between initial yielding and distance to the boundary in the Mo Σ3 bicrystal. The initial yield point is defined as the first excursion from elastic loading of at least 5 nm indentation depth. Close to the boundary, the yield load is reduced due to preferential nucleation at the grain boundary.

nucleation can be greatly affected by the presence of grain boundary steps. The present results can thus only provide a rough estimate of the extent of dislocation nucleation at grain boundaries.

A physical explanation of preferential nucleation at the boundary may be given by the grain boundary dislocation having a shear stress component on the slip plane, which assists the applied shear stress in generating a lattice dislocation loop. The maximum shear stress is attained at a distance of the width of the grain boundary dislocation, ξ. Assuming that nucleation of a dislocation loop occurs in the vicinity of the grain boundary when the total shear stress reaches a value of $\mu/2\pi$ as suggested by the experiments far away from the boundary, the applied shear stress necessary for nucleation becomes

$$\tau_a \approx \frac{\mu}{2\pi} - \frac{\mu b}{\pi(1-\nu)}\frac{1}{\xi}. \tag{7}$$

For the experimental value of $\tau_a = 2$ GPa, the width of the grain boundary dislocation is found to be $\xi = 0.9$ nm, which compares well to other estimates [34,35]. From Eq. (7), it follows that when the grain boundary dislocation core becomes more delocalized, the necessary nucleation shear stress at the grain boundary increases. As a consequence, localized cores at lower temperatures will act as stress concentrators, while at higher temperatures, the grain boundary dislocation cores become more spread and homogeneous nucleation near grain boundaries becomes less likely [35,36]. Of course it should be emphasized that the present results can only provide a rough estimate of the extent of dislocation nucleation at grain boundaries but evidently the mechanical response is completely different between these two bcc materials.

4.3. Predictive criteria for grain boundary yielding

When indentation-induced grain boundary yielding occurs, the boundary resistance to slip transfer can be quantitatively related to the strain bursts in a Hall–Petch type approach. This calculation and the relevant geometrical considerations have been addressed in more detail in a previous paper by the present authors [4]. In short, the dislocation pile-up is confined to a small distance d by the grain boundary on the one side and the indenter on the other side. Slip transfer occurs when the shear stress at the boundary reaches a critical value τ^* given by [37–39]

$$\tau^* = m(\tau_a - \tau_0)\sqrt{\frac{d}{4r}}, \tag{8}$$

where τ_a is the applied shear stress, τ_0 is the intrinsic frictional shear stress and r is the distance to the dislocation source in the adjacent grain. The factor m represents the misorientation between the slip systems on either side of the boundary. Rewriting Eq. (8) and setting $k_y = 2m^{-1}\tau^*\sqrt{r}$ gives the Hall–Petch equation

$$\tau_a = \tau_0 + \frac{k_y}{\sqrt{d}}. \tag{9}$$

A further analysis of the Hall–Petch slope k_y has recently been presented in [40]. With τ_a given by the CSM data, $\tau_0 = 200$ MPa and $d = d_{burst}$ as listed in Table 2, the Hall–Petch slope for the Fe–Si boundary is found to be $k_y = 0.63\ \mathrm{MNm}^{-3/2}$ with a standard

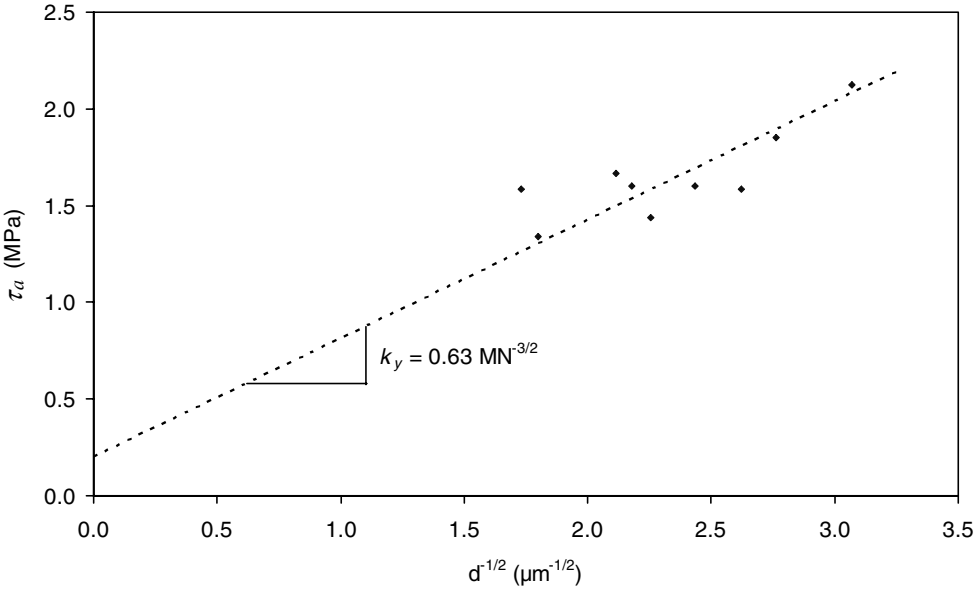

Fig. 8. Representation of the Fe–Si boundary yield events in a Hall–Petch type plot, i.e., with the applied shear stress plotted vs. the inverse square root of the distance to the boundary. The dashed line shows the fit to Eq. (9) assuming a frictional shear stress of $\tau_0 = 200$ MPa.

deviation of 0.09 $\mathrm{MNm}^{-3/2}$. Following Eq. (9), Fig. 8 shows a plot of the applied shear stress versus the inverse square root of the distance to the boundary for the observed yield events. Although the distances at which boundary yielding was observed do not span such a large range as to conclusively validate the $d^{-1/2}$ dependence of the shear stress, the results appear to be in general agreement with the proposed Hall–Petch type relation. Moreover, the resulting Hall–Petch slope $k_y = 0.63\ \mathrm{MNm}^{-3/2}$ compares well to the macroscopic value for α-Fe, $k_y = 0.583\ \mathrm{MNm}^{-3/2}$ [41,42]. Similar agreement was found by Wang and Ngan [5] for indentations at grain boundaries in niobium.

Indentation at submicrometer length scales may lead to appreciable strain gradients and produce size effects, which cannot be justified by classical theories of plasticity [12,43]. In our experiments, we found that the stress at which the boundary yields increases significantly when the indenter to boundary distance becomes smaller than 150 nm (see Table 2; the interfacial yield stress is roughly equal to one-third of the measured hardness). In other words, the boundary appears to be stronger when the probed volume becomes dimensionally constrained. In forthcoming papers, it is shown that this type of size effect can be accounted for by incorporating an interfacial energy term into gradient plasticity theory [44,45]. The experimentally observed dislocation transference phenomenon is similar to grain boundary yielding in a strain-gradient plasticity framework which allows interfaces to follow their own yield behavior. The analytical expressions derived in [46] predict that the interfacial yield stress increases as the specimen size decreases. In the present experimental observations, considering the specimen size to be the distance bounded between the indenter tip and grain boundary allows new type of size effects to be obtained through nanoindentation. It should be emphasized that a similar size dependence is not noted for the grain interior yielding, which was constantly observed at a load of approximately 50 μN. Any gradient plasticity approach is based on averaging dislocation densities in a certain volume. This approach becomes questionable when the volume is small and discrete dislocations govern the material behavior. In the mathematical treatment [44–46], an interfacial energy γ term connected to interfacial yielding and a length scale ℓ appear. By making a comparison with a dislocation description, it was found that γ can be viewed as an effective modulus of the interface depending on the number of geometrically stored dislocations, which are distributed over a certain length scale, ℓ, in front of the interface. In the present case, 80% of the dislocations are positioned over the length scale ℓ near the boundary and therefore a good relationship between discrete dislocations and gradient plasticity theory could be made at these volume sizes [44,45].

Beyond 150 nm from the boundary, the size effect is not appreciable and we can use the dislocation-based approach described above to predict grain boundary yielding. Table 3 lists the relevant properties of the grain boundaries investigated in this study and by Wang et al. The macroscopic Hall–Petch slope values k_y are consistent with the observations of slip transfer. In molybdenum, having the highest k_y value and thus the highest resistance to slip transfer, dislocations piled-up at the grain boundary but did not cross over to the adjacent

Table 3
Relevant parameters for the occurrence of grain boundary yielding during indentation

Material	H–P slope k_y ($MNm^{-3/2}$)	Closest slip system orientation m'	Activated slip system orientation m	Grain boundary yielding observed
Mo	0.78 [47]	1.00 (Σ3) 0.99 (Σ11)	0.78 (Σ3) 0.25 (Σ11)	No
Fe–Si	0.58 [42]	0.93	0.82	Yes, depending on indenter orientation
Nb [5]	0.19	0.90–0.99	–	Yes, regardless of indenter orientation

grain. The Hall–Petch slope for Fe–Si is lower; in this case, the boundary only yielded when faced by one side of the indenter. In the experiments by Wang et al. on niobium, having the lowest k_y value, grain boundary yielding was observed irrespective of the azimuthal orientation of the indenter, which they did not take into account. The effect of the indenter orientation on the boundary yielding can be understood by approximating the stress field by uniaxial pressure components perpendicular to the faces of the indenter, and recognizing that the resolved shear stress at the grain boundary is a maximum when one side is facing the boundary.

Besides the intrinsic resistance to slip transfer as quantified by the macroscopic value of the Hall–Petch slope, the ease of slip transmission is largely determined by the geometry of the experiment and the relative orientation of the slip systems. Wang et al. found that in niobium, strain bursts are observed for boundaries with $m' > 0.9$, where m' is given by

$$m' = \cos\theta_A \cos\theta_B \tag{10}$$

and θ_A and θ_B are, respectively, the angles between the closest slip planes on opposite sides of the boundary and the closest slip directions on these planes. However, this approach does not take the orientation of the grain boundary plane into account. Moreover, the closest available slip systems are not necessarily those activated during deformation, since slip proceeds mainly on systems for which the resolved shear stress is highest. A better description of the misorientation is therefore obtained by comparing only the maximum resolved shear stress (MRSS) slip systems in the indented grain with the available slip systems in the adjacent grain. To find the MRSS slip systems we assume a uniaxial compressive stress perpendicular to the surface of the indenter as mentioned before, and use Schmid behavior as a first approximation. The favored slip system in the adjacent grain can subsequently be found by maximizing the orientation factor m [48] given by

$$m = (\bar{L}_1 \cdot \bar{L}_2) * (\bar{g}_1 \cdot \bar{g}_2), \tag{11}$$

where $\bar{L}_1$ and $\bar{L}_2$ are the normalized intersection lines common to the slip planes and the boundary plane, and $\bar{g}_1$ and $\bar{g}_2$ are the normalized slip directions in the pile-up and emission grains, so that $m = 1$ for identical slip systems as in Eq. (10). Although the Mo Σ3 boundary has two perfectly aligned slip systems on either side ($m' = 1$), slip transmission from the MRSS slip system is relatively difficult ($m = 0.78$) as shown in Table 3. This difficulty in slip propagation was confirmed by in situ straining of Σ3 symmetric tilt boundaries [20,21], which showed that the dislocation–grain boundary interaction strongly depends on the orientation of the tensile axis with respect to the boundary plane.

5. Conclusions

We have characterized the mechanical response to nanoindentation of three bcc bicrystals as a function of the distance to the boundary. Hardening was found within 1 μm of all three boundaries due to pile-up of dislocations. Indentations close to the boundary in the Fe–Si bicrystal showed a characteristic yield excursion, which is attributed to slip transmission. This is supported by a comparison between the energy released during the excursion and the calculated interaction energy of the piled-up dislocations. Furthermore, new types of nanoindentation size effects are obtained by relating the hardness at the onset of this excursion to the distance of the indenter tip to the grain boundary [13,48].

The boundary resistance to slip transfer can be quantitatively related to the yield excursions by a Hall–Petch type calculation. By regarding the distance between the indenter and the boundary at the onset of slip transmission as representative for the slip pile-up, we obtain a Hall–Petch slope k_y that corresponds well to macroscopically determined values. Accordingly, it is shown that materials with higher k_y values exhibit increasing difficulty in slip transmission across boundaries. The Hall–Petch slope is therefore considered the most important parameter predicting the occurrence of the observed yield excursions. For materials with $k_y > 0.7\ MNm^{-3/2}$, slip transmission is not expected under Berkovich indentation.

Incipient plasticity during indentation of single crystals is often characterized by one or more yield excursions, which are attributed to the nucleation and multiplication of dislocations under the indenter. In this study, we found that these yield excursions are significantly suppressed for indentations close to a grain boundary, presumably due to easy dislocation nucleation at the boundary. The maximum distance at which grain boundary proximity affects the initial plasticity

was found to be of the order of the tip radius of the indenter.

Acknowledgments

The authors thank Pavel Lejcek and Tomas Vystavel for providing the bicrystal specimens. This work was funded by the Netherlands Institute for Metals Research under Project Number MC4.01104. K.E.A. acknowledges the US National Science Foundation for its support through the Graduate Research Fellowship Program.

References

[1] Westbrook JH, Aust KT. Acta Metall 1963;11:1151.
[2] Aust KT, Hanneman RE, Niessen P, Westbrook JH. Acta Metall 1968;16:291.
[3] Soifer YM, Verdyan A, Kazakevich M, Rabkin E. Scripta Mater 2002;47:799.
[4] Soer WA, De Hosson JTM. Mater Lett [in press].
[5] Wang MG, Ngan AHW. J Mater Res 2004;19:2478.
[6] Arzt E. Acta Mater 1998;46:5611.
[7] Choi Y, Van Vliet KJ, Li J, Suresh S. J Appl Phys 2003;94:6050.
[8] Lejcek P. Anal Chim Acta 1994;297:165.
[9] Pénisson JM, Vystavel T. Acta Mater 2000;48:3303.
[10] Vystavel T. PhD thesis. Université J. Fourier, Grenoble, 1999.
[11] Oliver WC, Pharr GM. J Mater Res 1992;7:1564.
[12] Nix WD, Gao H. J Mech Phys Solids 1998;46:411.
[13] Gerberich WW, Nelson JC, Lilleodden ET, Anderson P, Wyrobek JT. Acta Mater 1996;44:3585.
[14] Bahr DF, Kramer DE, Gerberich WW. Acta Mater 1998;46:3605.
[15] Kramer DE, Yoder KB, Gerberich WW. Philos Mag A 2001;81:2033.
[16] Eshelby JD, Frank FC, Nabarro FRN. Philos Mag 1951;42:351.
[17] Nabarro FRN, Basinski ZS, Holt DB. Adv Phys 1964;13:193.
[18] Gouldstone A, Koh HJ, Zeng KY, Giannakopoulos AE, Suresh S. Acta Mater 2000;48:2277.
[19] Shen Z, Wagoner RH, Clark WAT. Acta Metall 1988;36:3231.
[20] Lagow BW, Robertson IM, Jouiad M, Lassila DH, Lee TC, Birnbaum HK. Mater Sci Eng A 2001;309–310:445.
[21] Gemperlová J, Jacques A, Gemperle A, Vystavel T, Zárubová N, Janecek M. Mater Sci Eng A 2002;324:183.
[22] Gemperle A, Gemperlová J, Zárubová N. Mater Sci Eng A 2004;387–389:46.
[23] Vystavěl T, Jacques A, Gemperle A, Gemperlová J, George A. Mater Sci Forum 1999;294–296:397.
[24] Vitek V. Prog Mater Sci 1992;36:1.
[25] Duesbery MS. In: Nabarro FRN, editor. Dislocations in solids, vol. 8. Amsterdam: North-Holland; 2003. p. 67.
[26] Ito K, Vitek V. Philos Mag 2001;81:1387.
[27] Corcoran SG, Colton RJ, Lilleodden ET, Gerberich WW. Phys Rev B 1997;55:R16057.
[28] Larsson PL, Giannakopoulos AE, Söderlund E, Rowcliffe DJ, Vestergaard R. Int J Solids Struct 1996;33:221.
[29] Johnson KL. Contact mechanics. Cambridge University Press; 1985.
[30] Picu RC. J Comput-Aided Mater Des 2000;7:77.
[31] Khalfallah O, Condat M, Priester L. Philos Mag A 1993;67:231.
[32] Saraev D, Schmauder S. Phys Stat Sol B 2003;240:81.
[33] Lilleodden ET, Zimmerman JA, Foiles SM, Nix WD. J Mech Phys Solids 2003;51:901.
[34] Murr LE. Appl Phys Lett 1974;14:1974.
[35] Varin RA, Wyrzykowski JW, Lojkowski W, Grabski MW. Phys Stat Sol A 1978;45:565.
[36] Gleiter H. Mater Sci Eng 1982;52:91.
[37] Petch NJ. J Iron Steel Inst 1953;174:25.
[38] Hall EO. Proc Phys Soc 1951;B64:747.
[39] Hirth JP, Lothe J. Theory of dislocations. New York, NY: McGraw Hill; 1968.
[40] Bata V, Pereloma E. Acta Mater 2004;52:657.
[41] Courtney TH. Mechanical behavior of materials. New York, NY: McGraw Hill; 1990. p. 169.
[42] Anderson E, King DLW, Spreadborough J. Trans Metall Soc AIME 1968;242:115.
[43] Tymiak NI, Kramer DE, Bahr DF, Wyrobek TJ, Gerberich WW. Acta Mater 2001;49:1021.
[44] Aifantis KE, Soer WA, De Hosson JTM, Willis, JR. Rev Adv Mat Sci [submitted].
[45] Aifantis KE, De Hosson JTM, Willis JR. Int J Plast [in press].
[46] Aifantis KE, Willis JR. J Mech Phys Solids 2005;53:1049.
[47] Yoder KB, Elmustafa AA, Lin JC, Hoffman RA, Stone DS. J Phys: D Appl Phys 2003;36:884.
[48] Shen Z, Wagoner RH, Clark WAT. Scripta Metall 1986;20:921.